

Contents lists available at ScienceDirect

Case Studies in Construction Materials

journal homepage: www.elsevier.com/locate/cscm



Case study



Hybrid-fiber-reinforced strain-hardening ultra-high-performance concrete (SH-UHPC) with recycled fine aggregates

Rui-Yang Ma ^a, Zhi-Liang Zhang ^{a,b,*}, Jing-Hao Wei ^c, Feng-Yi Zhuo ^c, Han Zhang ^a, Fan Jiang ^d, Xiao-Hua Ji ^c, Yi-Nong Shen ^{e,f}, Ji-Xiang Zhu ^{g,**}

- ^a Institute of Advanced Engineering Structures, Zhejiang University, Hangzhou, China
- ^b School of Resources and Civil Engineering, Northeastern University, Shenyang, China
- ^c College of Civil Engineering and Architecture, Zhejiang University, Hangzhou, China
- ^d The Architectural Design & Research Institute of Zhejiang University, Hangzhou, China
- ^e School of Civil & Environmental Engineering and Geography Science, Ningbo University, Ningbo, China
- f Ningbo Key Laboratory of Energy Geostructure, Ningbo University, Ningbo, China
- g Department of Civil and Environmental Engineering, The Hong Kong Polytechnic University, Hong Kong

ARTICLE INFO

ABSTRACT

Keywords:
Strain-hardening ultra-high-performance concrete (SH-UHPC)
Recycled fine aggregates (RFA)
Hybrid fiber
Multiple cracking
C&D wastes

In order to increase environmental sustainability and to address the issue of construction and demolition (C&D) wastes accumulation, this study investigates the feasibility of using recycled fine aggregates (RFA) as a substitute to fully replace fine silica sand (FSS) in the production strainhardening ultra-high-performance concrete (SH-UHPC). Results showed that RFA-based SH-UHPC with hybrid fiber reinforcement achieved comparable compressive strength (over 100 MPa), and an impressive enhancement on tensile ductility by 68.3 %. Microstructural analyses via SEM, X-CT and microhardness test revealed that due to the lower intrinsic hardness of RFA more internal cracks were observed RFA-based SH-UHPC, indicating the role of RFA as active flaws in high strength matrix of SH-UHPC resulting in more saturated multiple cracking and enhanced strain-hardening behavior. In the end, the strategic utilization of RFA not only improves mechanical performance but also lowers overall environmental impacts, which highlights the sustainable and effective use of C&D wastes for developing greener high-performance construction materials.

1. Introduction

Over the past three decades, concrete construction has made several landmark advances in new material technologies [1–5], including ultra-high-performance concrete (UHPC) [6–36] and Engineered Cementitious Composites (ECC) [12–20]. UHPC is represented by a dense and discontinuous pore structure that reduces defects and mass transport in concrete, significantly improving its compressive strength, tensile strength and durability, making it suitable for construction applications in marine environment [21–23]. Although steel fiber was typically incorporated in UHPC to improve its ductility, the tensile strain capacity of UHPC is low (normally

E-mail addresses: ruiyangma@zju.edu.cn (R.-Y. Ma), zhiliangzhang@zju.edu.cn (Z.-L. Zhang), jinghaowei@zju.edu.cn (J.-H. Wei), zhuofengyi@zju.edu.cn (F.-Y. Zhuo), 12212095@zju.edu.cn (H. Zhang), zuadr_jf@163.com (F. Jiang), jixiaohua@zju.edu.cn (X.-H. Ji), shenyinong@nbu.edu.cn (Y.-N. Shen), ji-xiang.zhu@connect.polyu.hk (J.-X. Zhu).

https://doi.org/10.1016/j.cscm.2025.e04869

Received 29 April 2025; Received in revised form 29 May 2025; Accepted 31 May 2025 Available online 31 May 2025

2214-5095/© 2025 The Authors. Published by Elsevier Ltd. This is an open access article under the CC BY license (http://creativecommons.org/licenses/by/4.0/).

^{*} Corresponding author at: Institute of Advanced Engineering Structures, Zhejiang University, Hangzhou, China.

^{**} Corresponding author.

below 1.0 %) along with weak strain-hardening behavior [8,24–27]. ECC are a branch of fiber-reinforced cementitious materials that exhibit unique tensile strain-hardening behavior along with multiple-cracking properties [28–35]. Designed based on micromechanical principles, the excellent ductility (normally over 3 %) and crack control ability (less than 100 µm) of ECC were achieved through incorporating high-performance fibers including Polyvinyl Alcohol (PVA) fibers, and Polyethylene (PE) fibers, which can be crucial for construction materials exposed to harsh marine environments. In recent years, to achieve both high strength and high ductility of cementitious composites, Strain-Hardening Ultra-High-Performance Concrete (SH-UHPC) have been successfully designed and developed by combining the UHPC technology and the micromechanics-based design method of ECC [36]. Unlike conventional concrete that is brittle and prone to cracking [37–39], the incorporation of high-performance fibers (e.g., steel fiber, PE fiber or both) endows SH-UHPC with exceptional mechanical performance and durability, making it an ideal candidate for marine applications where resistance to corrosive seawater and extreme weather conditions is significant. However, both UHPC and ECC require the fine silica sand (FSS) with particle size less than 300 µm for achieving the targeted performance, which is non-renewable and expensive [40–43]. To achieve sustainability improvement of SH-UHPC, alternative aggregates including sea sand, river sand, coral sand, recycled fine aggregates and artificial aggregates have been used for greener production [44–47].

Among various available sources for alternative aggregates, the use of construction and demolition (C&D) wastes as both fine and coarse aggregates has gained widespread attention in recent years [48–50]. Compared with natural aggregate, recycled aggregate (RA) from further crushing of such wastes exhibits lower intrinsic density and porous structure due to the existing of old mortar, which leads to a weaker interfacial transition zone (ITZ) and consequently poorer mechanical performance [51–54]. Evangelista and de Brito [55] investigated the substitution of natural fine aggregates with recycled aggregates (up to a 100 % replacement ratio) and result showed that as the replacement ratio increased, there was a noticeable decline in overall mechanical performance. Despite the detrimental impact of RA on the mechanical performance of concrete, very recent efforts are seen in the development of UHPC with high/ultra-high compressive strength using recycled fine aggregates (RFA) to partially or even fully replace the natural aggregates [56–58]. On the other hand, recent studies have demonstrated that the incorporation of suitable artificial flaws including RFA can tailor the multiple cracking behavior of ECC, leading to improved strain-hardening characteristics [35,59–61]. Hence, the incorporation of RFA for producing SH-UHPC in this study aims to achieve several potential advantages including tailoring tensile performance of SH-UHPC and enhancing material sustainability.

Against the above background, the effect of fiber hybridization on the mechanical performance and cracking behavior of SH-UHPC was investigated, while SH-UHPC with fine silica sand was used as control group. Mechanical tests including uniaxial compressive test and direct tensile tests were conducted. The microstructures of SH-UHPC matrix were analyzed based on results of microhardness test, Backscattered Electron (BSE) with Energy Dispersive Spectroscopy (EDS) and X-ray computed tomography (X-CT) tests. Finally, the analysis of environmental impacts and cost efficiency of developed SH-UHPC was conducted to evaluate its commercial potential.

2. Experimental programs

2.1. Raw materials and mix proportion

The mix proportions (Table 1) of SH-UHPC included P·O 52.5 ordinary Portland cement, silica fume (SiO₂ content over 92 %), water, and polycarboxylate-based super-plasticizer (SP). FSS with an average particle size less than 300 μ m and RFA with an average particle size less than 1.18 mm were adopted as fine aggregate. The water/cementitious binder ratio was kept 0.2, the aggregate/binder ratio was kept at 0.3, and the SP/binder ratio was kept 0.013. In this study, hybrid fiber including steel and PE fibers were used for the production of SH-UHPC with a total fiber content of 2.0 % [32]. The properties of fibers are listed in Table 2.

2.2. Preparations of RA-based SH-UHPC with hybrid fibers

SH-UHPC specimens were prepared through a standardized mixing sequence (Fig. 1): initially, dry materials (i.e., cement, silica fume, and fine aggregates) were mixed in a planetary mixer for 5 minutes. Subsequently, aqueous phase components (water and superplasticizer) were added and blended for an additional 5-minute interval. Subsequently, steel fibers and PE fibers were incrementally introduced during the five-minute mixing to ensure homogeneous dispersion uniformity, followed by mold casting of the composite mixture. The cast specimens underwent initial curing at $20 \pm 1^{\circ}$ C for 48 hours prior to demolding, followed by standard moist curing (20°C, RH>95%) until 28-day testing age. The specimen nomenclature follows a logical coding system where, for

Table 1Mix proportions (by weight) and specimen IDs of SH-UHPC.

Raw Materials	S1.0P1.0-S	S1.0P1.0-R		S1.5 P0.5-R	S2.0P0.0-R
Dry Aggregate	Fine Silica Recycled	Fine Aggregate			
	Sand (0.300)	(0.300)			
Cement	0.800				
Silica Fume	0.200				
Water	0.200				
SP (in Solid)	0.013				
Steel Fibers (by vol.)	1.0 %	1.0 %	1.5 %	2.0 %	
PE Fibers (by vol.)	1.0 %	1.0 %	0.5 %	0.0 %	

Table 2Geometries and properties of straight steel and PE fibers.

Fiber	Diameter (µm)	Length (mm)	Strength (MPa)	Modulus (GPa)	Density (g/cm ³)
Steel fiber	115	8	≥ 3000	200	7.9
PE fiber	24	12	3000	100	0.97

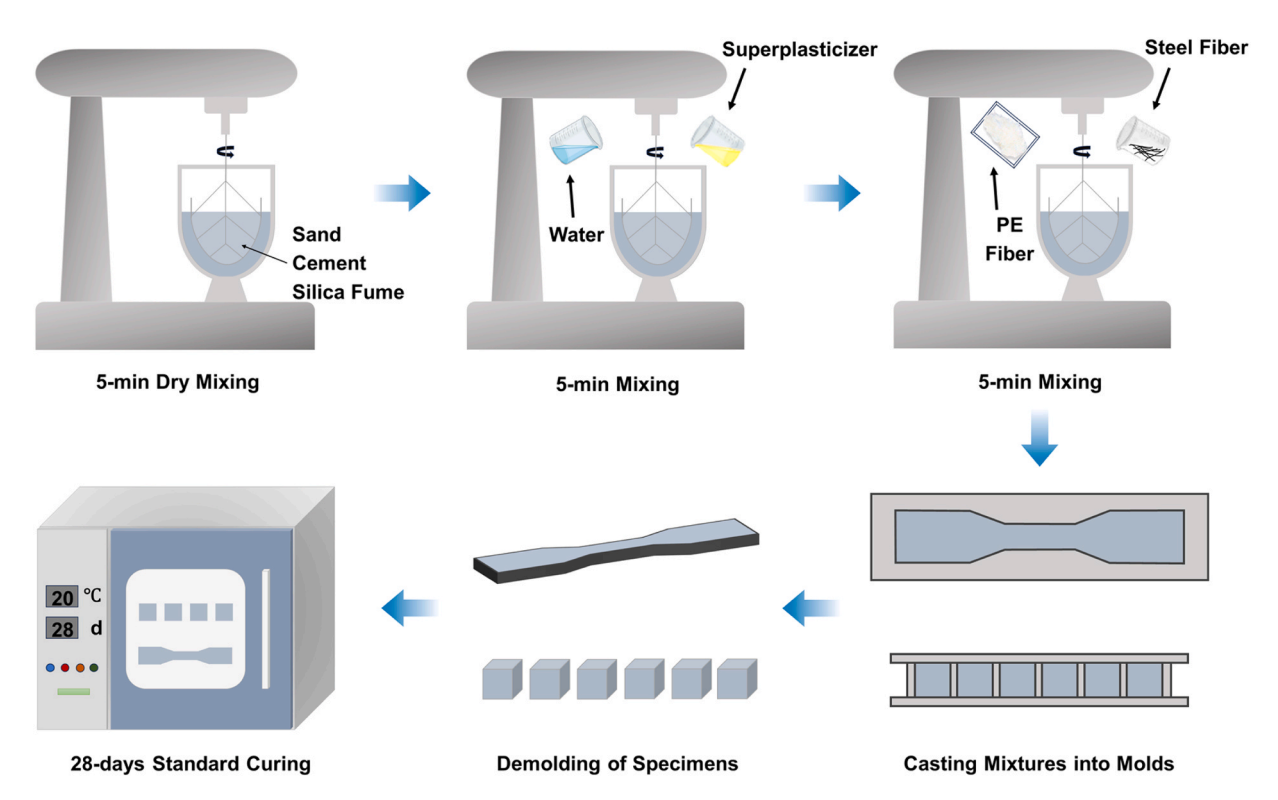


Fig. 1. Preparations of SH-UHPC and testing procedure.

instance, S1.0P1.0-R indicates: "\$1.0" means containing steel fibers with 1.0 % volume fraction, "P1.0" means that containing PE fibers with 1.0 % volume fraction, and the last letter "R" represents the recycled fine aggregates (RFA)

2.3. Testing programs

Compression tests were conducted in accordance with ASTM C109/C109M [62] standards. Three standard cubic specimens (50 mm \times 50 mm \times 50 mm) from each specimen designation were subjected to compressive loading using a universal compression testing machine, with a controlled loading rate of 1.0 MPa/s.

Direct tensile tests were conducted in accordance with ASTM C307–16 [63] standard. Three dumbbell-shaped specimens from each designation were tested using an electromechanical universal testing machine under displacement control mode with a quasi-static tensile loading rate of 0.50 mm/s. Two high-precision linear variable differential transformers (LVDTs) were mounted on the sides of the SH-UHPC specimens to accurately measure axial deformation within an 80 mm gauge length. Prior to formal testing, speckle patterns were created on the specimen surfaces through spray painting to enable strain field measurement via digital image correlation (DIC) technology. During the tests, digital images were captured every 3 s, and the image resolution was approximately 15 µm per

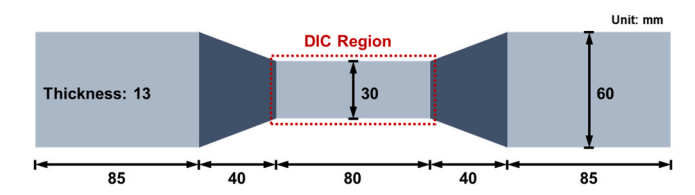


Fig. 2. Dimensions of direct tensile specimens.

pixel. High-resolution digital cameras systematically captured images of the monitoring area to comprehensively track the deformation behavior of SH-UHPC, as shown in Fig. 2.

For backscattered electron (BSE) microscopic analysis, representative samples of S1.0P1.0-S and S1.0P1.0-R were carefully extracted from dumbbell-shaped specimens using precision cutting techniques. After ultrasonic cleaning in acetone (40 kHz, 15 min), the specimens were embedded in epoxy resin: positioned at the center of molds, filled with low-viscosity epoxy resin, and subjected to vacuum degassing to eliminate bubbles, followed by 24 h curing. Subsequently, both samples underwent a series of polishing steps using an automatic grinding/polishing machine to achieve optimal surface flatness and parallelism. To enhance conductivity for imaging, a thin gold layer was uniformly coated on the polished surfaces via sputter coating. BSE imaging was performed at $600 \times \text{magnification}$ to comprehensively observe microstructural characteristics. For the S1.0P1.0-R sample, EDS elemental mapping was synchronously conducted to characterize and distinguish various phases based on elemental distributions, with a focus on Ca, Si, Al, Fe, and C.

The specimen preparation procedure for microhardness testing strictly followed the BSE-EDS standard methodology, with the sole exception of omitting the gold sputter coating. Representative specimens of S1.0P1.0-S and S1.0P1.0-R were selected for investigation. To address the multiphase composite characteristics of RFA, micro-Vickers hardness testing was conducted to comparatively evaluate RFA constituents (natural aggregates and old mortar) and FSS, focusing on the old mortar-new matrix interface, the RFA/matrix interfacial transition zone (ITZ) at 20 μ m proximity, with its adjacent hydrated matrix phase spanning 50 μ m outward in the RFA-based UHPC. Forty indentation points per phase were systematically measured with a grid spacing of 50 μ m. All experimental data points were included in the fitting process to ensure the reliability and accuracy of the resulting curve.

To systematically analyze the failure mechanisms of hybrid fiber-reinforced SH-UHPC, high-resolution digital imaging systems were employed to macroscopically characterize the fracture surfaces of S1.0P1.0-S, S1.0P1.0-R, S1.5P0.5-R, and S2.0P0.0-R specimens after direct tensile failure. For representative mixes S1.0P1.0-S and S1.0P1.0-R, small-sized samples were extracted from the fracture surfaces of post-tensioned specimens. These samples were then subjected to micro-morphological characterization using a scanning

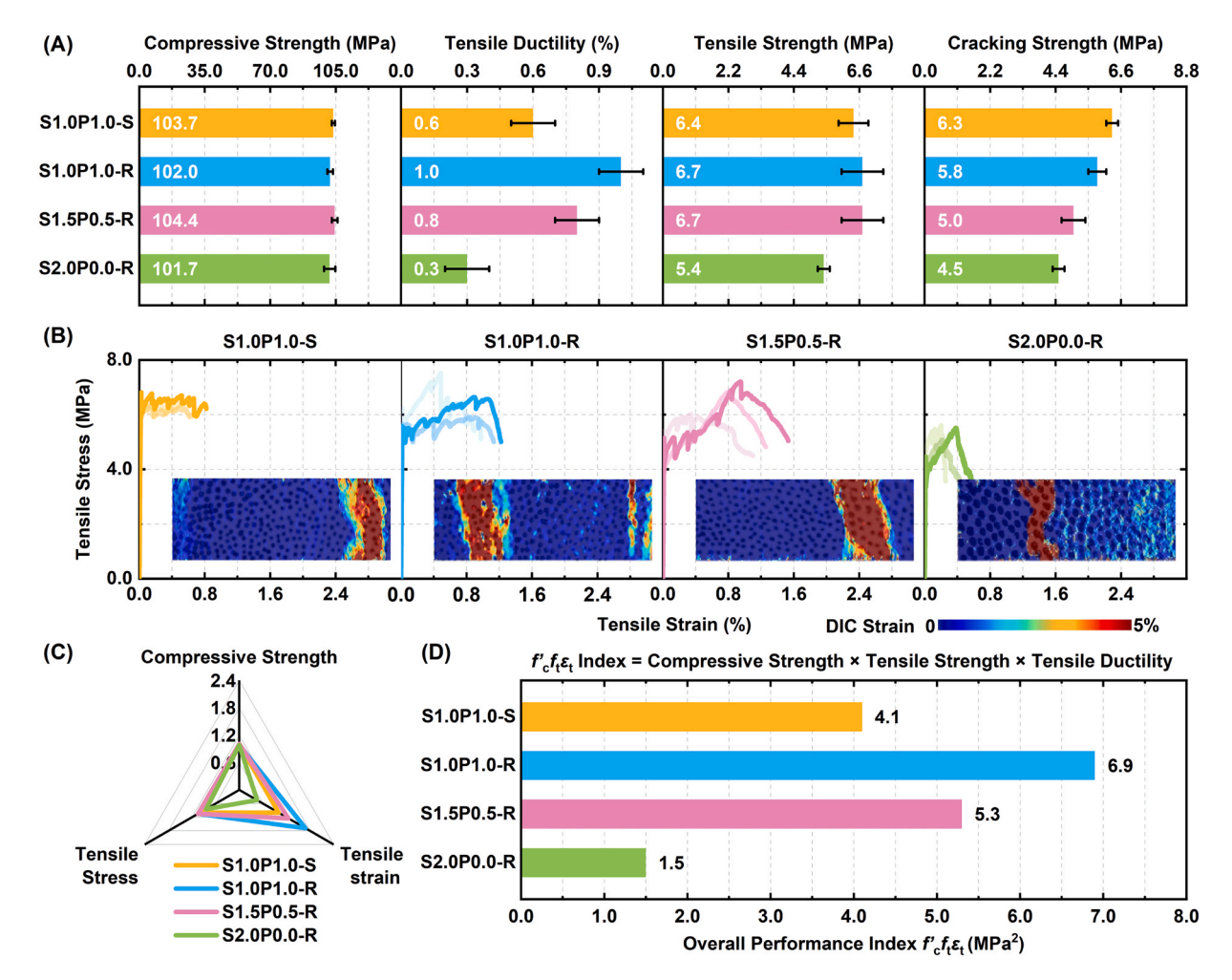


Fig. 3. Mechanical properties of SH-UHPC of different aggregate types and hybrid fiber dosages: (A) Mechanical properties; (B) Tensile stress-strain curves and DIC patterns; (C) Three-dimensional assessment of mechanical performances; and (D) $f_c f_t \epsilon_t$ Index.

electron microscope under 15 kV accelerating voltage and 10 mm working distance to analyze fiber failure modes.

Finally, representative samples were extracted from the central regions of fractured dumbbell-shaped specimens (S1.0P1.0-S, S1.0P1.0-R, S1.5P0.5-R, S2.0P0.0-R) after direct tensile testing. These samples were subjected to high-resolution three-dimensional tomographic scanning using a micro-focus X-CT system operating at a voxel resolution of $10.5 \, \mu m$. The Feldkamp-Davis-Kress (FDK) reconstruction algorithm was employed to achieve detailed visualization of internal crack patterns.

3. Mechanical properties

3.1. Compressive strength

The compression properties of SH-UHPC with various aggregates and fiber hybridization were present in Fig. 3A, and all specimens exhibit 28-day compressive strengths exceeding 100 MPa. In general, the effect of fiber hybridization and aggregate type had marginal effect on the compressive strength of SH-UHPC (ranging from 101.7 MPa to 104.4 MPa), indicating the feasibility of using RFA in the production of SH-UHPC.

3.2. Tensile performance

The tensile behavior for SH-UHPC are illustrated in Fig. 3, with a summary of mechanical properties provided in Table 3. As depicted in Fig. 3B, all tested mix designs exhibit strain-hardening behavior in tension. For the hybrid fiber dosage series, the tensile strengths ranged from 6.4 MPa to 6.7 MPa with minor variation. Compared to mix with steel fiber (i.e., S2.0P0.0-R), the mixes incorporating polyethylene (PE) fibers (i.e., S1.0P1.0-R, S1.5P0.5-R and S1.0P1.0-S) showed relatively higher tensile strengths. On the other hand, as the content of PE fiber content decreased and steel fiber content increased, SH-UHPC exhibited reduced tensile strain capacity. When RFA was used to replace FSS, the tensile strain capacity increased by 66.7 % from 0.6 % (i.e., S1.0P1.0-S) to 1.0 % (i.e., S1.0P1.0-R) due to the reduction of matrix cracking strength (see Fig. 3A). This is because the introduction of RFA worked as additional flaws in the high strength matrix [31] resulting in enhanced multiple cracking. The crack patterns and DIC results of SH-UHPC at the peak strain are presented in Fig. 3B. It can be seen that S2.0P0.0-R with 2 % steel fiber showed localized cracking behavior, and large sections of dumbbell specimens remained uncracked. In addition, the mixes with hybrid fiber system exhibited more saturated cracking behavior.

3.3. Evaluation of overall performance

A three-dimensional assessment of mechanical performance including compression strength f_c ', tensile ductility ε_b and tension strength f_t were conducted (see Fig. 3C). The combination of these three indicators reflects the overall mechanical performance including strength and ductility of SH-UHPC. In Fig. 3C, compared with SH-UHPC using FSS, those with RFA showed enhanced tensile ductility and strength, while their compressive strength present insignificant change. In addition, the increasing of steel fiber content led to decreased tensile ductility, whereas compressive strength was slightly changed.

The $f'c_l \epsilon_t$ Index [32] was introduced to quantitatively characterize the mechanical performance of SH-UHPC (results shown in Fig. 3D). Among all mixes, the S2.0P0.0-R exhibits the lowest $f'c_l \epsilon_t$ Index (1.6 MPa²). In contrast, for the hybrid fiber dosage series, the $f'c_l \epsilon_t$ Index increases with PE fiber content, reaching 5.6 MPa² and 6.8 MPa² for S1.5P0.5-R and S1.0P1.0-R, respectively. Substituting RFA with FSS significantly reduced the index to 4.0 MPa² (i.e., S1.0P1.0-S), further demonstrating the feasibility of using RFA as fine aggregate to improve the overall mechanical properties of SH-UHPC.

3.4. Fracture surface and microhardness

Fig. 4 presents the SEM images of fiber surface (see Fig. 4A) and fiber failure modes (Fig. 4B and C). Fig. 4B demonstrates two typical failure modes of PE fibers: pull-out failure and fracture failure. Fig. 4C present the surface morphology of steel fiber and pull-out failure was observed. SEM analysis revealed significantly fewer hydration products at the steel fiber interface compared to the scratched PE fiber surfaces, suggesting weaker bonding with the SH-UHPC matrix.

To investigate the interface properties between RFA and SH-UHPC matrix, micro-Vickers hardness testing was conducted. The Weibull distribution model was employed to fit the microhardness data of each phase, with fitting results presented in Table 4. Notably, "20 μ m from the interface" and "50 μ m from the interface" in the table denote test regions located 20 μ m and 50 μ m away from

Table 3
Mechanical properties of SH-UHPC.

Mechanical Properties	S1.0P1.0-S	S1.0P1.0-R	S1.5P0.5-R	S2.0P0.0-R
Compressive Strength, f'c (MPa)	103.7 ± 0.8	102.0 ± 1.5	104.4 ± 1.5	101.7 ± 3.0
Tensile Ductility, ε_t (%)	0.6 ± 0.1	1.0 ± 0.1	0.8 ± 0.1	0.3 ± 0.1
Ultimate Tensile Strength, f_t (MPa)	6.4 ± 0.5	6.7 ± 0.7	6.7 ± 0.7	$\textbf{5.4} \pm \textbf{0.2}$
Tensile Cracking Strength, f_{tc} (MPa)	6.3 ± 0.2	5.8 ± 0.3	5.0 ± 0.4	4.5 ± 0.2
$f'_t f_t \varepsilon_t \operatorname{Index} (MPa^2)$	4.0	6.8	5.6	1.6

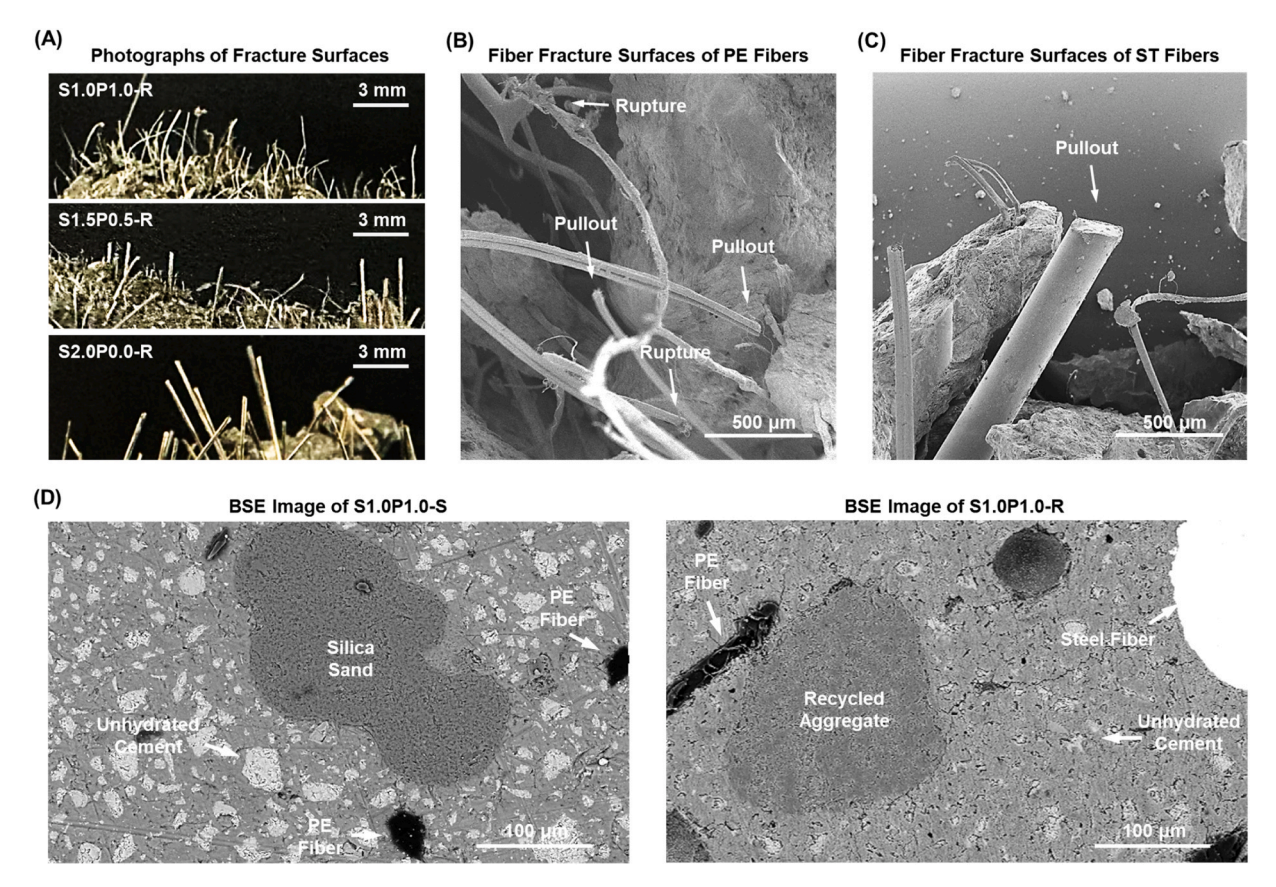


Fig. 4. Microscopic evaluations of SH-UHPC: (A) Photographs of fracture surfaces of S1.0P1.0-R, S1.5P0.5-R and S2.0P0.0-R; (B) Fiber Fracture Surfaces of PE Fibers; (C) Fiber Fracture Surfaces of ST Fibers; (D) BSE images of S1.0P1.0-S and S1.0P1.0-R.

the RFA/matrix interface, representing the ITZ of RA-based UHPC and the extended cementitious matrix region, respectively, with spatial positioning accuracy controlled within \pm 1 μ m. The correlation coefficients for all phases are as high as 0.99, suggesting that the microhardness of different phases follows a Weibull distribution.

Fig. 5 presents the Weibull probability plots of phase-specific microhardness distributions in SH-UHPC. The experimental data demonstrate that natural aggregates (i.e., FSS and natural aggregates within RFA) exhibit significantly higher microhardness than other phases. Specifically, FSS achieves the highest average microhardness (1502.6 HV) due to its superior silica purity (SiO₂ \geq 92 %), while the natural aggregates in RFA show slightly lower microhardness (1147.5 HV). Despite the old mortar in RFA exhibiting the lowest microhardness (46.0 HV), which substantially reduces the overall hardness of RFA, the compressive strength of RFA-based SH-UHPC remains comparable to that of FSS-based SH-UHPC (see Fig. 3A), this behavior is systematically analyzed in Section 4.2. Additionally, the microhardness values for the bulk matrix (20 and 50 μ m from the interface) are 128.8 HV and 158.6 HV, respectively, with the hardness of old mortar/new matrix interface further decreasing to 104.2 HV. Therefore, the old mortar with lowest hardness may reduce the matrix fracture toughness and act as additional crack propagation paths, resulting in enhanced the strain-hardening behavior of SH-UHPC, which aligned with the DIC patterns shown in Fig. 3B.

 Table 4

 Microhardness values of different areas in the matrix.

Testing Areas	Fitted Distributions	Correlation Coefficient	Mean Value (HV)
Fine Silica Sand (FSS)	$F(x) = 1 - \exp(-(x/1534.4)^26.1)$	0.99	1502.6
Aggregate in RFA	$F(x) = 1-\exp(-(x/1193.9)^11.0)$	0.99	1147.5
Old Mortar in RFA	$F(x) = 1 - \exp(-(x/48.0)^{11.9})$	0.99	46.0
Interface between Old Mortar and New matrix	$F(x) = 1-\exp(-(x/107.9)^{15.2})$	0.99	104.2
20 μm from Interface	$F(x) = 1-\exp(-(x/131.9)^22.6)$	0.99	128.8
50 μm from Interface	$F(x) = 1 - \exp(-(x/163.1)^{19.3})$	0.99	158.6

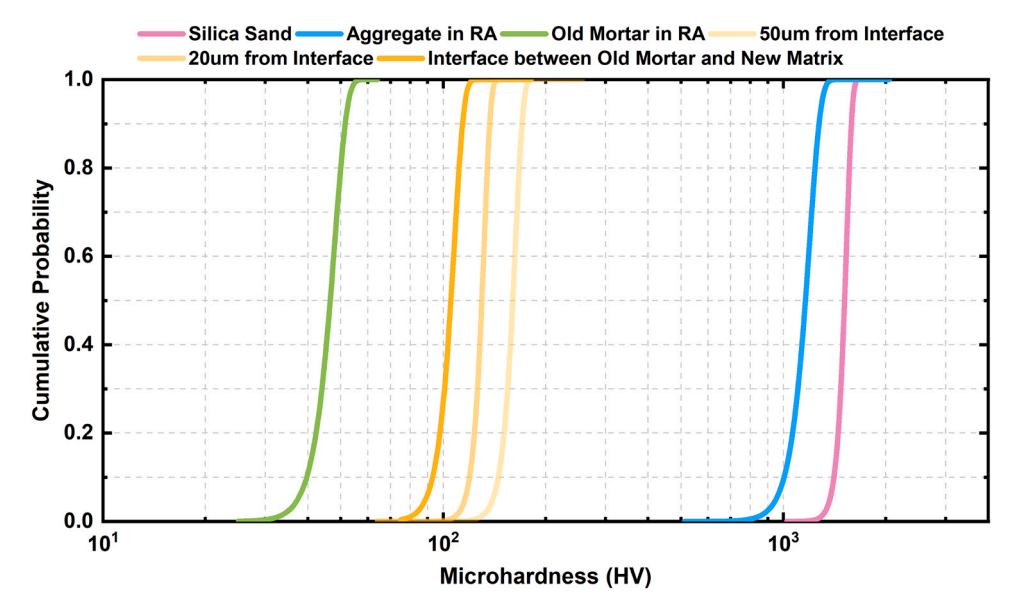


Fig. 5. Cumulative frequency distributions of microhardness measurements in SH-UHPC's different phases.

3.5. BSE-EDS results

Fig. 4D presents the microstructures of S1.0P1.0-R obtained from BSE images, where unreacted cement (i.e., bright white angular particles) were observed due to its low water-to-cement ratio. Compared to S1.0P1.0-S, less unreacted cement were formed in SH-UHPC with RFA as fine aggregate, which is in line with the high compressive strength of mixes with recycled aggregate. This observation is consistent with previous studies by Evangelista et al. [55], Salahuddin et al. [64] and Khatib, J. M. [65], which demonstrates comparable compressive strength in concrete materials when replacing natural fine aggregates with RFA.

Fig. 6A presents the BSE images of S1.0P1.0-R magnified at 1200 times and EDS analysis was conducted to obtain the element

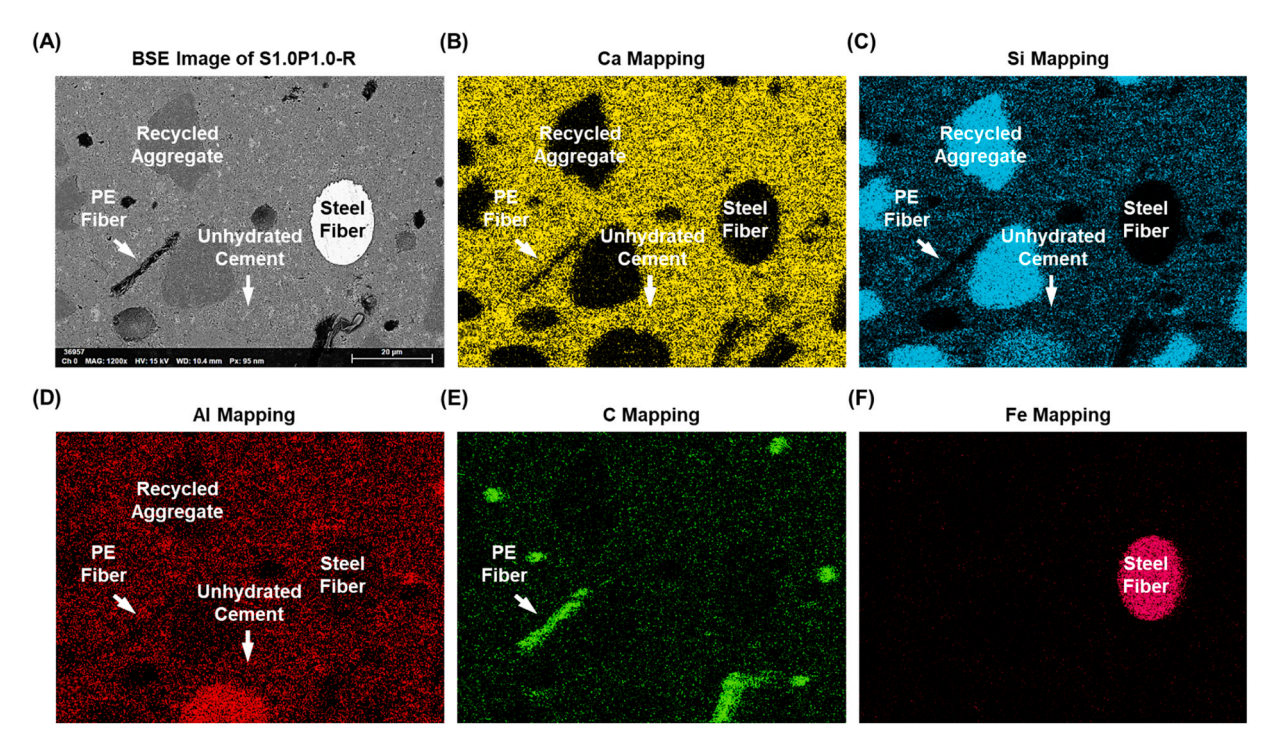


Fig. 6. BSE images of S1.0P1.0-R; (B) EDS mapping of Ca; (C) EDS mapping of Si; (D) EDS mapping of Al; (E) EDS mapping of C; (F) EDS mapping of Fe;.

distribution. A notably densified microstructure was observed in at the interface which was in accordance with the high compressive strength of RFA-based SH-UHPC. In Fig. 6B and D, the distribution of Calcium (Ca) and Aluminum (Al) appeared more pronounced in the matrix of SH-UHPC than in other phases, which is attributed to the cement used as primary binder material in the SH-UHPC production. In Fig. 6C, the distribution of Silicon (Si) can be used to identify the recycled aggregate. In addition, the presence of Carbon (C) elements and Iron (Fe) in Fig. 6E and F can also be used to identify the PE fiber and steel fiber, respectively.

3.6. X-CT results

The microstructures in SH-UHPC samples were investigated using X-ray micro-computed tomography (micro-CT), and the two-dimensional (2D) X-CT images of cracked SH-UHPC are present in Fig. 7. All slices were acquired from the mid-section scanning area of specimens, ensuring structural representativeness of the selected regions. Compared with S1.0P1.0-S, RFA-based SH-UHPC exhibited more internal cracking, which is attributed to the lower average microhardness of RFA compared to FSS allowing cracks to penetrate more easily through RFA. In Fig. 7B-D, the crack number increased with the increase of PE fiber content, which is in accordance with the crack patterns present in Fig. 3B. Furthermore, in Fig. 7, the black circles represented the initial flaws (i.e., pores) and the flaws penetrated by single or several cracks were considered as active flaws while those remained intact in the matrix were inactive flaws [66]. A comparative analysis of Fig. 7B-D indicates that variations in hybrid fiber dosage do not significantly affect the active-to-inactive flaw ratio.

4. Environmental and cost assessments

Beyond mechanical properties, the environmental impact and economic feasibility are essential criteria for assessing sustainable construction materials. Therefore, it is crucial to evaluate the characteristics of SH-UHPC from both environmental and economic perspectives. Table 5 presents the unit-mass embodied carbon emissions, energy consumption, and material costs associated with raw materials. The calculations for per-unit-volume embodied carbon, embodied energy, and cost of SH-UHPC were derived through cumulative summation of the products between material consumption per cubic meter and corresponding parameters in Table 5. The material's environmental impacts, costs, and mechanical properties are demonstrated in Table 6 and Fig. 8A. Furthermore, to evaluate the overall performance of SH-UHPC, a representative index considering compressive strength (f'c), tensile strength (ft) and tensile ductility (ϵt) were adopted and embodied carbon, embodied energy and cost per index were compared in Fig. 8B.

4.1. Embodied carbon

Embodied carbon refers to the total CO_2 emissions generated during material manufacturing, transportation, and construction processes. In Fig. 8A, the S1.0P1.0-R specimen achieves the lowest embodied carbon emissions, with reductions of 15.1 % and 0.2 % compared to the S2.0P0.0-R and S1.0P1.0-S specimens, respectively. This difference is primarily attributed to two key factors: the high carbon footprint of steel fibers during its production, and the reduced carbon emissions by substituting natural aggregates with recycled aggregates. Notably, when evaluating the carbon emissions intensity per $f'c_1c_1$ Index (as shown in Fig. 8B), the S1.0P1.0-R specimen exhibits even more pronounced reductions of 80.0 % and 41.3 % in embodied carbon emissions compared to the S2.0P0.0-R and S1.0P1.0-S specimens, respectively, owing to its superior mechanical performance.

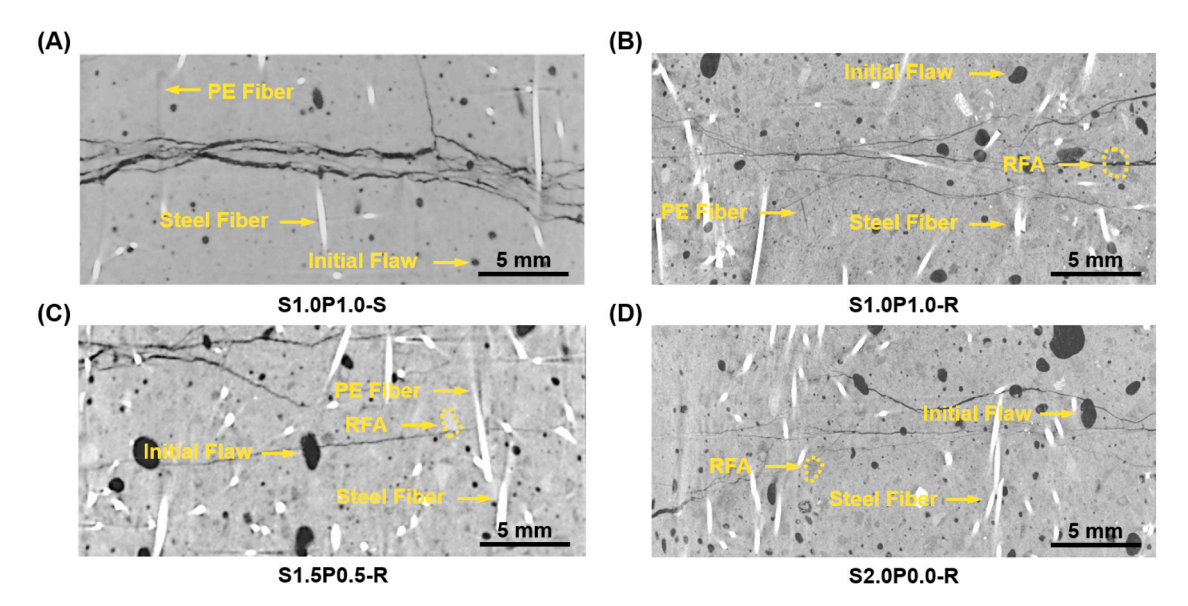


Fig. 7. X-CT images: (A) S1.0P1.0-S; (B) S1.0P1.0-R; (C) S1.5P0.5-S; (D) S2.0P0.0-S.

Table 5Embodied carbon, embodied energy, and costs of raw materials in matrices.

Raw Materials	Embodied Carbon [(kg CO ₂)/kg]	Embodied Energy (MJ/kg)	Cost* (CNY/kg)
Cement	0.912 [67]	5.500 [68]	0.460 [69]
Silica Fume (SF)	0.024 [70]	0.100 [68]	2.000 [69]
Fine Silica Sand (FSS)	0.023 [71]	0.067 [72]	0.800 [73]
Recycled Fine Aggregate (RFA)	0.012 [74]	0.0034 [74]	0.062 [75]
Super-plasticizer (SP, Solid)	1.880 [67]	11.470 [68]	51.000 [69]
Water	0.001 [72]	0.100 [72]	0.004 [69]
PE Fiber	2.000 [76]	94.500 [76]	170.000 [76]
Steel Fiber	2.830 [68]	36.000 [68]	12.320 [68]

^{*} HKD/CNY = 0.88 for Steel Fiber in [68].

Table 6Estimated embodied carbon, embodied energy, and material costs of SH-UHPC materials.

Environmental and Cost Assessments	S1.0P1.0-S	S1.0P1.0-R	S1.5P0.5-R	S2.0P0.0-R
$f' c_t \varepsilon_t$ Index (MPa ²)	4.0	6.8	5.6	1.6
Embodied Carbon (kg CO ₂ /m ³)	1232.1	1228.6	1336.4	1447.1
Embodied Energy (MJ/m ³)	9713.9	9692.6	10,690.7	11,706.4
Material Costs (CNY/m³)	3849.2	3506.2	3011.5	2521.2
Embodied Carbon per $f' f_t \varepsilon_t$ Index (kg CO ₂ /m ³ / MPa ²)	308.0	180.7	238.6	904.4
Embodied Energy per $f'_{t}f_{t}\varepsilon_{t}$ Index $(MJ/m^{3}/MPa^{2})$	2428.5	1425.4	1909.1	7316.5
Material Costs per $f' J_t \varepsilon_t$ Index (CNY/m ³ / MPa ²)	962.3	515.6	537.8	1575.8

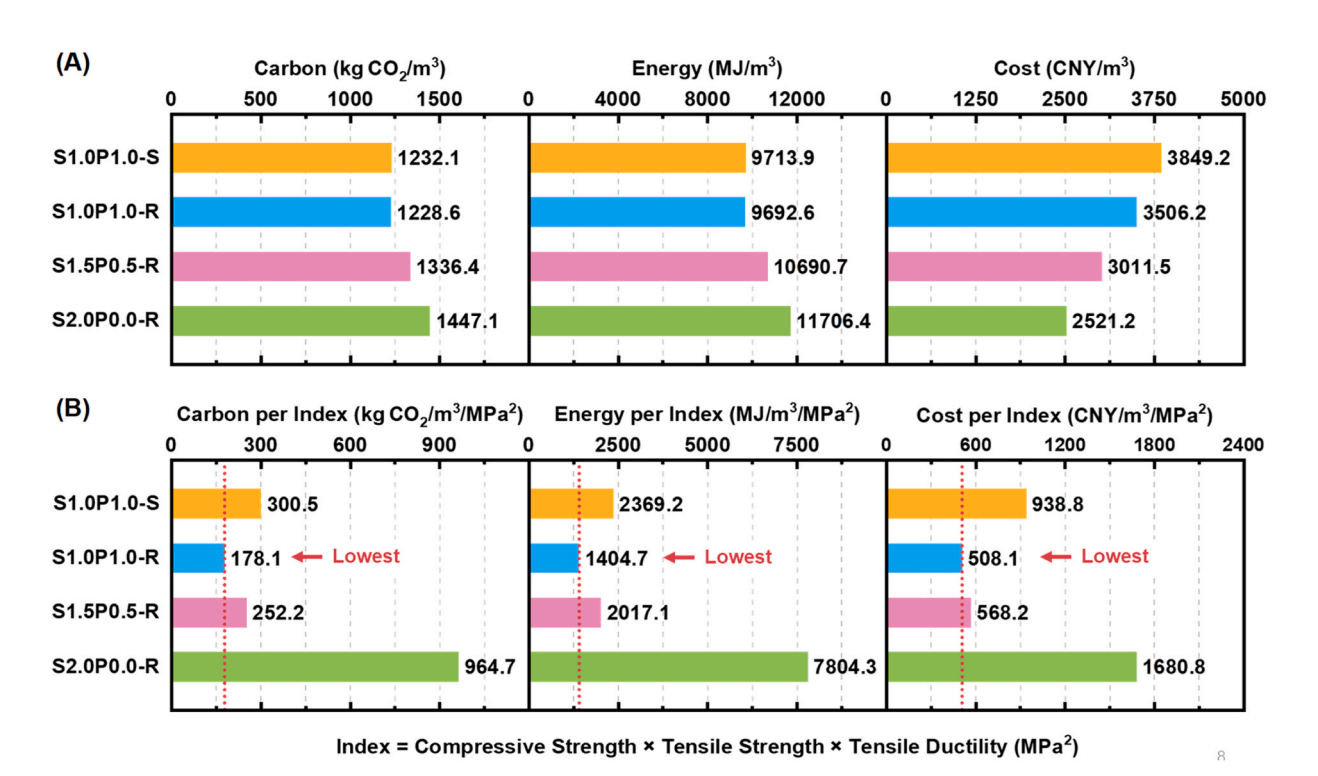


Fig. 8. Sustainability and cost assessments of SH-UHPC in this study: (A) Embodied carbon, embodied energy, and material cost; and (B) Embodied carbon per *f'cftet* Index, embodied energy per *f'cftet* Index, and material cost per *f'cftet* Index. S1.0P1.0-R showed the lowest embodied carbon, embodied energy, and material cost per *f'cftet* Index.

4.2. Embodied energy

Embodied energy refers to the total energy required during extraction, refining, transportation, and construction processes. Similar to embodied carbon, as shown in Fig. 8A-B, the S1.0P1.0-R specimen exhibits optimal energy performance, achieving the lowest embodied energy of $[9692.6 \text{ MJ/m}^3]$ for bulk volume and $[1425.4 \text{ MJ/m}^3/\text{MPa}^2]$ for per f' $f_t \varepsilon_t$ Index. These findings highlight that SH-UHPC with RFA and reduced steel fiber content can sustain excellent mechanical properties while enhancing sustainability.

4.3. Cost analysis

To assess the market potential of the developed SH-UHPC, cost analysis results are presented in Table 6 and Fig. 8A. Unlike embodied carbon and energy, the S2.0P0.0-R group with 2 % steel fiber volume fraction achieved the minimum material cost of [2521.2 CNY/m³] due to lower steel fiber unit price. Conversely, the hybrid fiber-reinforced S1.0P1.0-R group exhibited increased material cost of [3506.2 CNY/m³] owing to the high cost of PE fibers. However, benefiting from both greener raw materials and enhanced mechanical performance, the cost per $f' d_t e_t$ Index of S1.0P1.0-R decreased substantially by 67.3 % compared to S2.0P0.0-R, reaching the lowest value among all four mixtures, indicating the coupled greenness and high performance of the RFA-based SH-UHPC developed in this study.

5. Ductility enhancement mechanism

According to the design theory of strain-hardening cementitious composites (SHCC), the introduction of active defects is crucial for enhancing the ductility of SH-UHPC [77,78]. As mentioned in Section 4.3, RFA containing old mortar worked as "additional defects" in the SH-UHPC matrix. The old mortar regions in RFA reduce the fracture toughness of the matrix, preferentially serving as crack propagation paths under tensile loading. Furthermore, the ITZ of RFA and discontinuous structures (such as interfacial microcracks between RFA and matrix) provide additional crack initiation sites and create new pathways for multi-cracking behavior in SH-UHPC, thereby achieving more saturated multiple cracking in SH-UHPC and ultimately leading to enhanced tensile ductility. DIC strain field analysis confirms that compared with S1.0P1.0-S, the S1.0P1.0-R specimen exhibits more uniform crack distribution, demonstrating a typical saturated cracking pattern (see Fig. 3).

6. Conclusions

In this study, recycled fine aggregates (RFA) were adopted to produce strain-hardening ultra-high-performance concretes (SH-UHPC). Comprehensive investigation was conducted to study the effects of fiber hybridization and aggregate type on the mechanical properties and cost-effectiveness of the developed SH-UHPC. The principal conclusions are summarized as follows:

- The use of RFA as fine aggregate and hybrid fiber (i.e., steel fiber and PE fiber) had marginal impact on the compressive strength of SH-UHPC. For tensile performance, the addition of RFA resulted in enhanced tensile ductility by 68.3 % compared with SS-based SH-UHPC and the tensile strain capacity of SH-UHPC decreased with the increase of steel fiber content.
- XCT results revealed that RFA in SH-UHPC can potentially work as active flaws due to the lower average microhardness of RFA
 compared to FSS, which resulted in more saturated multiple cracking and higher tensile ductility.
- The environmental and economic assessment indicated that S1.0P1.0-R demonstrated superior overall performance including carbon emissions per $f' d_t e_t$ Index, energy consumption per $f' d_t e_t$ Index, and cost efficiency per $f' d_t e_t$ Index. Due to the greenness of recycled aggregate and higher mechanical performance, the adoption of RFA as fine aggregate in the development of SH-UHPC can lead to maximum reductions of 41.3 % in both embodied carbon and embodied energy, and 46.4 % in cost per index.

This study focused on the feasibility of using RFA to produce SH-UHPC, but certain limitations remain. For example, studies on parameters such as aggregate content and the quantification of RFA aggregate as active flaws should be conducted in the future. Additionally, the durability and long-term mechanical performance of SH-UHPC with RFA were not investigated. Furthermore, the strain-hardening behavior of SH-UHPC was weak in this study and future research should investigate methods to enhance its strain-hardening behavior and tensile ductility. The environmental and economic assessments were conducted mainly based on the production phase of the materials. Future research should extend to a full life-cycle assessment considering construction, usage, and demolition phases.

CRediT authorship contribution statement

Fan Jiang: Writing – review & editing, Supervision. Xiao-Hua Ji: Supervision, Resources. Yi-Nong Shen: Writing – review & editing, Supervision, Funding acquisition. Zhi-Liang Zhang: Writing – review & editing, Visualization, Investigation, Formal analysis, Conceptualization. Jing-Hao Wei: Investigation, Formal analysis. Feng-Yi Zhuo: Investigation, Formal analysis. Han Zhang: Writing – review & editing, Funding acquisition. Ji-Xiang Zhu: Writing – review & editing, Supervision, Resources, Conceptualization. Rui-Yang Ma: Writing – original draft, Visualization, Investigation, Data curation.

Declaration of Competing Interest

The authors declare that they have no known competing financial interests or personal relationships that could have appeared to influence the work reported in this paper.

Acknowledgements

The authors would like to acknowledge the support of the National Natural Science Foundation of China (Nos. 523B2090 and 52408272), Ningbo Natural Science Foundation (No. 2024J089), and the International Sci-tech Cooperation Projects under the "Innovation Yongjiang 2035" Key R&D Programme (No. 2024H019).

Data availability

Data will be made available on request.

References

- [1] F. Liu, Y. Li, J. Lv, Y. Liu, H. Li, F. Mu, Uniaxial compression performance of SIFCON with the arc-shaped steel fibers, J. Build. Eng. 100 (2025) 111678.
- [2] P. Duxson, A. Fernández-Jiménez, J.L. Provis, G.C. Lukey, A. Palomo, J.S. van Deventer, Geopolymer technology: the current state of the art, J. Mater. Sci. 42 (2007) 2917–2933.
- [3] J.C. Lao, R.Y. Ma, L.Y. Xu, Y. Li, Y.N. Shen, J. Yao, B.T. Huang, Fly ash-dominated high-strength engineered/strain-hardening geopolymer composites (HS-EGC/SHGC): influence of alkalinity and environmental assessment, J. Clean. Prod. 447 (2024) 141182.
- [4] L.Y. Xu, J.C. Lao, L.P. Qian, M. Khan, T.Y. Xie, B.T. Huang, Low-carbon high-strength engineered geopolymer composites (HS-EGC) with full-volume fly ash precursor; role of silica modulus, J. CO2 Util. 88 (2024) 102948.
- [5] J.C. Lao, B.T. Huang, Y. Fang, L.Y. Xu, J.G. Dai, S.P. Shah, Strain-hardening alkali-activated fly ash/slag composites with ultra-high compressive strength and ultra-high tensile ductility, Cem. Concr. Res. 165 (2023) 107075.
- [6] P. Richard, M. Chevrezy, Composition of reactive powder concretes, Cem. Concr. Res. 25 (7) (1995) 1501–1511.
- [7] K. Wille, A.E. Naaman, S. El-Tawil, G.J. Parra-Montesinos, Ultra-high performance concrete and fiber reinforced concrete: achieving strength and ductility without heat curing, Mater. Struct. 45 (3) (2012) 309–324.
- [8] K. Wille, S. El-Tawil, A.E. Naaman, Properties of strain hardening ultra high performance fiber reinforced concrete (UHP-FRC) under direct tensile loading, Cem. Concr. Compos. 48 (2014) 53–66.
- [9] M.J. Kim, D.Y. Yoo, Y.S. Yoon, Effects of geometry and hybrid ratio of steel and polyethylene fibers on the mechanical performance of ultra-high-performance fiber-reinforced cementitious composites, J. Mater. Res. Technol. 8 (2) (2019) 1835–1848.
- [10] X. Shen, E. Brühwiler, Influence of local fiber distribution on tensile behavior of strain hardening UHPFRC using NDT and DIC, Cem. Concr. Res. 132 (2020) 106042.
- [11] Z. Fang, Y. Xiang, Z. Kuang, C.L. Wang, Fatigue properties of reactive powder concrete with different steel fiber ratios, J. Hunan Univ. (Nat. Sci.) 38 (6) (2011) 6–12.
- [12] V.C. Li, Engineered Cementitious Composites (ECC) Bendable Concrete for Sustainable and Resilient Infrastructure. Verlag GmbH Germany, Springer, Berlin, Heidelberg, 2019.
- [13] S. Wang, V.C. Li, Engineered cementitious composites with high-volume fly ash, Acids Mater. J. -Am. Concr. Inst. 104 (3) (2007) 233-241.
- [14] D. Zhang, J. Yu, H. Wu, B. Jaworska, B.R. Ellis, V.C. Li, Discontinuous micro-fibers as intrinsic reinforcement for ductile Engineered Cementitious Composites (ECC), Compos. Part B: Eng. 184 (2020) 107741.
- [15] C.K. Leung, Design criteria for pseudoductile fiber-reinforced composites, J. Eng. Mech. 122 (1) (1996) 10–18.
- [16] L.Y. Xu, J. Yu, B.T. Huang, J.C. Lao, H.L. Wu, X. Jiang, J.G. Dai, Green and LOw-carbon Matrices for Engineered/strain-hardening Cementitious Composites (ECC/SHCC): towards sustainable and resilient infrastructure, J. Clean. Prod. (2025) 144968.
- [17] B.T. Huang, J.Q. Wu, J. Yu, J.G. Dai, C.K. Leung, V.C. Li, Seawater sea-sand engineered/strain-hardening cementitious composites (ECC/SHCC): assessment and modeling of crack characteristics, Cem. Concr. Res. 140 (2021) 106292.
- [18] Y. Liu, W.Z. Wu, Y.X. Zhang, W. Hou, H. Zhang, L.G. Peng, Engineered/strain-hardening cementitious composites (ECC/SHCC) for resilient cold-region infrastructure: a critical review of freeze-thaw durability, Case Stud. Constr. Mater. (2025) e04362.
- [19] J.X. Zhu, L.Y. Xu, B.T. Huang, K.F. Weng, J.G. Dai, Recent developments in engineered/strain-hardening cementitious composites (ECC/SHCC) with high and ultra-high strength, Constr. Build. Mater. 342 (2022) 127956.
- [20] Y.X. Zhang, Y.H. Gao, R. Lin, W. Hou, G.W. Yan, J.R. Lan, B.T. Huang, Tuning superior hydrophobic performance of Engineered/Strain-Hardening Cementitious Composites (ECC/SHCC) via polydimethylsiloxane-based bulk modification, Mater. Des. (2025) 114117.
- [21] J. Li, Z. Wu, C. Shi, Q. Yuan, Z. Zhang, Durability of ultra-high performance concrete—a review, Constr. Build. Mater. 255 (2020) 119296.
- [22] R. Yu, P. Spiesz, H.J.H. Brouwers, Mix design and properties assessment of ultra-high performance fibre reinforced concrete (UHPFRC), Cem. Concr. Res. 56 (2014) 29–39.
- [23] K. Habel, M. Viviani, E. Denarié, E. Brühwiler, Development of the mechanical properties of an ultra-high performance fiber reinforced concrete (UHPFRC), Cem. Concr. Res. 36 (7) (2006) 1362–1370.
- [24] S.T. Kang, Y. Lee, Y.D. Park, J.K. Kim, Tensile fracture properties of an Ultra High Performance Fiber Reinforced Concrete (UHPFRC) with steel fiber, Compos. Struct. 92 (1) (2010) 61–71.
- [25] Z. Shi, Q. Su, F. Kavoura, M. Veljkovic, Uniaxial tensile response and tensile constitutive model of ultra-high performance concrete containing coarse aggregate (CA-UHPC), Cem. Concr. Compos. 136 (2023) 104878.
- [26] Y.X. Zhang, Q. Zhang, L.Y. Xu, W. Hou, Y.S. Miao, Y. Liu, B.T. Huang, Transfer learning for intelligent design of lightweight Strain-Hardening Ultra-High-Performance Concrete (SH-UHPC), Autom. Constr. 175 (2025) 106241.
- [27] B.T. Huang, Z.L. Zhang, H. Xi, T. Zhang, M. Chen, J.H. Wei, L.Y. Xu, Strain-hardening ultra-high-performance concrete (SH-UHPC) with hybrid steel and polyethylene fibers: enhanced tensile ductility at subzero temperatures, Theor. Appl. Fract. Mech. (2025) 104987.
- [28] J. Yao, C.K. Leung, A new physical model for empirical fiber snubbing effect in cementitious composites based on large deflection beam theory, Cem. Concr. Compos. 96 (2019) 238–251.
- [29] J. Yu, C. Lu, Y. Chen, C.K.Y. Leung, Experimental determination of crack-bridging constitutive relations of hybrid-fiber strain-hardening cementitious composites using digital image processing, Constr. Build. Mater. 173 (2018) 359–367.
- [30] J.X. Zhu, K.F. Weng, W.H. Liu, B.T. Huang, K.D. Peng, J.H. Zhu, J.G. Dai, Thin-layer ultra-high-strength engineered cementitious composites (UHS-ECC) reinforced with small-diameter FRP bars for structural strengthening, Thin Walled Struct. 205 (2024) 112592.
- [31] L.Y. Xu, B.T. Huang, J.C. Lao, J. Yao, V.C. Li, J.G. Dai, Tensile over-saturated cracking of ultra-high-strength engineered cementitious composites (UHS-ECC) with artificial geopolymer aggregates, Cem. Concr. Compos. 136 (2023) 104896.

- [32] B.T. Huang, J.X. Zhu, K.F. Weng, V.C. Li, J.G. Dai, Ultra-high-strength engineered/strain-hardening cementitious composites (ECC/SHCC): material design and effect of fiber hybridization, Cem. Concr. Compos. 129 (2022) 104464.
- [33] D. Huang, S. Zong, Z. Liu, S. Li, Axial tensile properties of PVA fiber reinforced recycled geopolymer concrete, J. Inn. Mong. Univ. Technol. (Nat. Sci. Ed.) 3 (2023) 265–272.
- [34] X. Qiu, W. Chen, L. Li, H. Li, H. Li, H. Liu, The effects of particle sizes of expanded perlite on the mechanical properties and chloride penetration resistance of ECCs, J. Build. Eng. 78 (2023) 107706.
- [35] Q.H. Li, S.Y. Zhao, B.T. Huang, L.Y. Xu, S.L. Xu, Simultaneous enhancement of ductility and sustainability of high-strength Strain-Hardening Cementitious Composites (SHCC) using recycled fine aggregates, J. Clean. Prod. 470 (2024) 143357.
- [36] K.F. Weng, J.X. Zhu, B.T. Huang, J.G. Dai, J.F. Chen, Interfacial shear behavior between prefabricated strain-hardening ultra-high-performance concrete (SH-UHPC) and cast-in-place concrete, Eng. Struct. 325 (2025) 119405.
- [37] F. Gong, X. Sun, Y. Takahashi, K. Maekawa, W. Jin, Computational modeling of combined frost damage and alkali-silica reaction on the durability and fatigue life of RC bridge decks, J. Intell. Constr. 1 (1) (2023) 1–14.
- [38] X. Sun, S. Wang, J. Jin, Z. Wang, F. Gong, Computational methods of mass transport in concrete under stress and crack conditions: a review, J. Intell. Constr. 1 (2) (2023) 1–20.
- [39] X. Zhu, H. Abe, D. Hayashi, H. Tanaka, Behavioral characteristics of RC beams with non-uniform corrosion along the reinforcement, J. Intell. Constr. 1 (3) (2023) 1–21.
- [40] Y. Li, J. Li, E.H. Yang, X. Guan, Investigation of matrix cracking properties of engineered cementitious composites (ECCs) incorporating river sands, Cem. Concr. Compos. 123 (2021) 104204.
- [41] J.G. Teng, Y. Xiang, T. Yu, Z. Fang, Development and mechanical behaviour of ultra-high-performance seawater sea-sand concrete, Adv. Struct. Eng. 22 (14) (2019) 3100–3120.
- [42] X. Duan, J. Chen, C. Yan, C. Sun, J. Zhang, Effect of steel slag on hydration of belite sulphoaluminate cement from solid waste, J. Inn. Mong. Univ. Technol. (Nat. Sci. Ed.) 6 (2023) 549–554.
- [43] Q. Gao, L. Liu, X. Song, R. Bai, Enhancing strength of cement solidified Zn2+ and phenol contaminated soil with slag geopolymer, J. Inn. Mong. Univ. Technol. (Nat. Sci. Ed.) 1 (2024) 77–81.
- [44] B.T. Huang, J.Q. Wu, J. Yu, J.G. Dai, C.K. Leung, High-strength seawater sea-sand engineered cementitious composites (SS-ECC): mechanical performance and probabilistic modeling, Cem. Concr. Compos. 114 (2020) 103740.
- [45] Y. Li, J. Li, E.H. Yang, X. Guan, Mechanism study of crack propagation in river sand Engineered Cementitious Composites (ECC), Cem. Concr. Compos. 128 (2022) 104434.
- [46] Y. Shi, H. Jing, B. Liu, C. Hou, H. Qian, Synergistic utilization of porous coral sand and fly ash for multifunctional engineered cementitious composites with polyethylene fibers: intensified electromagnetic wave absorption and mechanism, J. Clean. Prod. 396 (2023) 136497.
- [47] Y. Guan, C. Zou, Y. Kang, B. Yang, Mechanical properties and stress-strain constitutive models of desert sand concrete in different regions, J. Inn. Mong. Univ. Technol. (Nat. Sci. Ed.). 2024. 43(01) (63-69) (2024).
- [48] B. Wang, L. Yan, Q. Fu, B. Kasal, A comprehensive review on recycled aggregate and recycled aggregate concrete, Resour., Conserv. Recycl. 171 (2021) 105565.
- [49] S.M. Levy, P. Helene, Durability of recycled aggregates concrete: a safe way to sustainable development, Cem. Concr. Res. 34 (11) (2004) 1975–1980.
- [50] G. Bai, C. Zhu, C. Liu, B. Liu, An evaluation of the recycled aggregate characteristics and the recycled aggregate concrete mechanical properties, Constr. Build. Mater. 240 (2020) 117978.
- [51] C.S. Poon, Z.H. Shui, L. Lam, Effect of microstructure of ITZ on compressive strength of concrete prepared with recycled aggregates, Constr. Build. Mater. 18 (6) (2004) 461–468.
- [52] Y. Liu, P. Ren, N. Garcia-Troncoso, K.H. Mo, T.C. Ling, Roles of enhanced ITZ in improving the mechanical properties of concrete prepared with different types of recycled aggregates, J. Build. Eng. 60 (2022) 105197.
- [53] D. Kong, T. Lei, J. Zheng, C. Ma, J. Jiang, J. Jiang, Effect and mechanism of surface-coating pozzalanics materials around aggregate on properties and ITZ microstructure of recycled aggregate concrete, Constr. Build. Mater. 24 (5) (2010) 701–708.
- [54] J. Liu, K. Ma, J. Shen, J. Zhu, G. Long, Y. Xie, B. Liu, Influence of recycled concrete aggregate enhancement methods on the change of microstructure of ITZs in recycled aggregate concrete, Constr. Build. Mater. 371 (2023) 130772.
- [55] L. Evangelista, J. De Brito, Mechanical behaviour of concrete made with fine recycled concrete aggregates, Cem. Concr. Compos. 29 (5) (2007) 397-401.
- [56] M. Amin, I.Y. Hakeem, A.M. Zeyad, B.A. Tayeh, A.M. Maglad, I.S. Agwa, Influence of recycled aggregates and carbon nanofibres on properties of ultra-high-performance concrete under elevated temperatures, Case Stud. Constr. Mater. 16 (2022) e01063.
- [57] Y. Leng, Y. Rui, S. Zhonghe, F. Dingqiang, W. Jinnan, Y. Yonghuan, H. Xiang, Development of an environmental Ultra-High Performance Concrete (UHPC) incorporating carbonated recycled coarse aggregate, Constr. Build. Mater. 362 (2023) 129657.
- [58] H. Zhang, T. Ji, X. Zeng, Z. Yang, X. Lin, Y. Liang, Mechanical behavior of ultra-high performance concrete (UHPC) using recycled fine aggregate cured under different conditions and the mechanism based on integrated microstructural parameters, Constr. Build. Mater. 192 (2018) 489–507.
- [59] H. Liu, J. Xiao, T. Ding, Flexural performance of 3D-printed composite beams with ECC and recycled fine aggregate concrete: experimental and numerical analysis, Eng. Struct. 283 (2023) 115865.
- [60] Y. Zhou, G. Gong, Y. Huang, C. Chen, D. Huang, Z. Chen, M. Guo, Feasibility of incorporating recycled fine aggregate in high performance green lightweight engineered cementitious composites, J. Clean. Prod. 280 (2021) 124445.
- [61] J. Li, E.H. Yang, Macroscopic and microstructural properties of engineered cementitious composites incorporating recycled concrete fines, Cem. Concr. Compos. 78 (2017) 33–42.
- [62] ASTM C109/C109M, Standard Test Method for Compressive Strength of Hydraulic Cement Mortars, ASTM International, West Conshohocken, PA, 2013.
- [63] ASTM C307-18, Standard test method for tensile strength of chemical-resistant mortar, grouts, and monolithic surfacings, Am. Soc. Test. Mater. 6 (02) (2018) 1–4.
- [64] H. Salahuddin, L.A. Qureshi, A. Nawaz, S.S. Raza, Effect of recycled fine aggregates on performance of Reactive Powder Concrete, Constr. Build. Mater. 243 (2020) 118223.
- [65] J.M. Khatib, Properties of concrete incorporating fine recycled aggregate, Cem. Concr. Res. 35 (4) (2005) 763-769.
- [66] L.Y. Xu, B.T. Huang, J.C. Lao, J.G. Dai, Tailoring strain-hardening behavior of high-strengtH Engineered Cementitious Composites (ECC) using hybrid silica sand and artificial geopolymer aggregates, Mater. Des. 220 (2022) 110876.
- [67] S. Zhang, Z. Li, B. Ghiassi, S. Yin, G. Ye, Fracture properties and microstructure formation of hardened alkali-activated slag/fly ash pastes, Cem. Concr. Res. 144 (2021) 106447.
- [68] J. Yu, Y. Chen, C.K. Leung, Mechanical performance of strain-hardening cementitious composites (SHCC) with hybrid polyvinyl alcohol and steel fibers, Compos. Struct. 226 (2019) 111198.
- [69] W.M. Shaban, K. Elbaz, J. Yang, B.S. Thomas, X. Shen, L. Li, Li, Effect of pozzolan slurries on recycled aggregate concrete: mechanical and durability performance, Constr. Build. Mater. 276 (2021) 121940.
- [70] N. Vijayarethinam, Silica fume applications, World Cem. 40 (2009) 97-100.
- [71] Y. Tang, J. Xiao, D. Wang, M. Zhang, Effect of carbonation treatment on fracture behavior of low-carbon mortar with recycled sand and recycled powder, Cem. Concr. Compos. 142 (2023) 105178.
- [72] J. Yu, H.L. Wu, C.K. Leung, Feasibility of using ultrahigh-volume limestone-calcined clay blend to develop sustainable medium-strength Engineered Cementitious Composites (ECC), J. Clean. Prod. 262 (2020) 121343.
- [73] L.Y. Xu, B.T. Huang, J.G. Dai, Development of engineered cementitious composites (ECC) using artificial fine aggregates, Constr. Build. Mater. 305 (2021) 124742.

- [74] D. Kumar, T. Mi, E.H. Yang, Improving the material sustainability of strain-hardening magnesium-silicate-hydrate composite by incorporating aggregates, Constr. Build. Mater. 407 (2023) 133576.
- [75] H.A. Shah, Q. Yuan, N. Photwichai, Use of materials to lower the cost of ultra-high-performance concrete-A review, Constr. Build. Mater. 327 (2022) 127045.
- [76] J.C. Lao, B.T. Huang, L.Y. Xu, M. Khan, Y. Fang, J.G. Dai, Seawater sea-sand engineered geopolymer composites (EGC) with high strength and high ductility, Cem. Concr. Compos. 138 (2023) 104998.
- [77] L.Y. Xu, B.T. Huang, Q. Lan-Ping, J.G. Dai, Enhancing long-term tensile performance of engineered cementitious composites (ECC) using sustainable artificial geopolymer aggregates, Cem. Concr. Compos. 133 (2022) 104676.
- [78] S. Wang, V.C. Li, Tailoring of pre-existing flaws in ECC matrix for saturated strain hardening, in: Proceedings of the FRAMCOS-5 (2004) 1005-1012.